NEOPLASIA
www.neoplasia.com

Volume 15 Number 11 November 2013 pp. 1218–1230 1218

# PTEN Phosphatase–Independent Maintenance of Glandular Morphology in a Predictive Colorectal Cancer Model System[1]

**Ishaan C. Jagan*,[2], Ravi K. Deevi*,[2], Aliya Fatehullah*,[2], Rebecca Topley*, Joshua Eves*, Michael Stevenson†, Maurice Loughrey‡,§, Kenneth Arthur*,§ and Frederick Charles Campbell***

*Centre for Cancer Research and Cell Biology, Queen's University of Belfast, Belfast, United Kingdom; †Centre for Public Health, Queen's University of Belfast, Belfast, United Kingdom; ‡Department of Histopathology, Royal Victoria Hospital, Belfast, United Kingdom; §Northern Ireland Molecular Pathology Laboratory, Centre for Cancer Research and Cell Biology, Queen's University, Belfast, United Kingdom

## Abstract

Organotypic models may provide mechanistic insight into colorectal cancer (CRC) morphology. Three-dimensional (3D) colorectal gland formation is regulated by phosphatase and tensin homologue deleted on chromosome 10 (PTEN) coupling of cell division cycle 42 (cdc42) to atypical protein kinase C (aPKC). This study investigated PTEN phosphatase-dependent and phosphatase-independent morphogenic functions in 3D models and assessed translational relevance in human studies. Isogenic PTEN-expressing or PTEN-deficient 3D colorectal cultures were used. In translational studies, apical aPKC activity readout was assessed against apical membrane (AM) orientation and gland morphology in 3D models and human CRC. We found that catalytically active or inactive PTEN constructs containing an intact C2 domain enhanced cdc42 activity, whereas mutants of the C2 domain calcium binding region 3 membrane-binding loop (M-CBR3) were ineffective. The isolated PTEN C2 domain (C2) accumulated in membrane fractions, but C2 M-CBR3 remained in cytosol. Transfection of C2 but not C2 M-CBR3 rescued defective AM orientation and 3D morphogenesis of PTEN-deficient Caco-2 cultures. The signal intensity of apical phospho-aPKC correlated with that of $Na^+/H^+$ exchanger regulatory factor-1 (NHERF-1) in the 3D model. Apical NHERF-1 intensity thus provided readout of apical aPKC activity and associated with glandular morphology in the model system and human colon. Low apical NHERF-1 intensity in CRC associated with disruption of glandular architecture, high cancer grade, and metastatic dissemination. We conclude that the membrane-binding function of the catalytically inert PTEN C2 domain influences cdc42/aPKC-dependent AM dynamics and gland formation in a highly relevant 3D CRC morphogenesis model system.

*Neoplasia (2013) 15, 1218–1230*

Abbreviations: aPKCζ, atypical protein kinase Cζ; CBR3, calcium binding region 3; cdc42, cell division cycle 42; EV, empty vector; GFP, green fluorescent protein; H&E, hematoxylin and eosin; NHERF-1, $Na^+/H^+$ exchanger regulatory factor-1; PTEN, phosphatase and tensin homologue deleted on chromosome 10; shRNA, short hairpin RNA; TBS, Tris/HCl-buffered saline; TNM, Tumor, Node, Metastasis; wt, wild type

Address all correspondence to: Frederick Charles Campbell, MD, Lisburn Rd, Belfast, Antrim BT96RF, United Kingdom. E-mail: f.c.campbell@qub.ac.uk

[1]The research was funded by the Wellcome Trust (grant WT081232MA) and Friends of the Cancer Centre (Belfast, United Kingdom). There are no competing interests or conflicts of interest.

[2]These authors contributed equally to this manuscript.

Received 11 September 2012; Revised 8 October 2013; Accepted 11 October 2013


DOI 10.1593/neo.121516

## Introduction

Colorectal cancer (CRC) is the third most common malignancy and the second most common cause of cancer death despite diagnostic and treatment advances [1]. All stages of CRC evolution from benign adenoma to invasive cancer involve dynamic alterations of glandular architecture, ranging from reorganization of polarized epithelium around a central lumen to complete glandular disruption [2]. Neoplastic deregulation of glandular morphogenesis may allow escape of tumor cells [3] or cell clusters from glandular structures that easily penetrate matrix barriers [4]. Histologic grading of these phenomena in human CRC has major prognostic significance [5].

Mechanistic insight into cancer morphology has been provided by fundamental studies in three-dimensional (3D) organotypic models [6,7]. Development and maintenance of glandular architecture involves coordinated assembly of a uniform apical membrane (AM) interface around a central lumen, guided by a correctly oriented mitotic spindle [6]. Spindle mispositioning promotes AM misassembly at ectopic sites, and subsequent enlargement of aberrant AM loci induces a vacuolar, multilumen phenotype [6]. Molecular regulators of spindle orientation also modulate apical junctional complexes implicated in cell-cell adhesion [8]. Defective spindle orientation may thus link AM dynamics [6] and junctional adhesion instability [9] implicated in glandular dysmorphogenesis and tumor cell escape from glands [10] during cancer progression.

Many tumor suppressors function by regulation of spindle orientation [11] and epithelial morphogenesis [12,13]. Deficiency of the phosphatase and tensin homologue deleted on chromosome 10 (PTEN) tumor suppressor associates with aberrant gland morphology in adenomas [14] and dysmorphic high-grade CRCs [15,16]. PTEN engages a highly conserved apical polarity pathway involving the GTPase cell division cycle 42 (cdc42) [7,17], interacting partitioning defective polarity (PAR) proteins and atypical protein kinase C (aPKC) [17,18] that regulates spindle orientation [19] and AM dynamics [20,21]. Disruption of cdc42/partitioning defective polarity signaling attenuates apical enrichment of aPKCζ and promotes spindle misorientation and glandular morphology defects [19]. We have shown that incomplete knockdown of PTEN in an isogenic Caco-2 organotypic model (Caco-2 ShPTEN cells) deregulates cdc42 and induces AM mispositioning and development of a multilumen, vacuolar phenotype evocative of high-grade cancer [7]. PTEN has phosphatase-dependent and phosphatase-independent functions [22], but neither oncogenic phosphatidylinositol 3-kinase signaling [23] nor phosphatidylinositol 3-kinase–modulating treatment [7] influenced AM coordination or Caco-2 gland development [7,23]. Relevant PTEN-dependent mechanisms thus remain unclear. While 3D Caco-2 models provide compelling insights into molecular regulation of AM orientation and glandular organization, clinical validation has been lacking.

To address these knowledge gaps, we investigated effects of distinct PTEN functional domains by transfection of wild-type (wt) PTEN and various catalytically active or inactive PTEN mutants. Effects were assessed on cdc42 activation and/or AM orientation and 3D Caco-2 glandular morphogenesis. Here, we show that the catalytically inert PTEN C2 domain enhanced cdc42 activity and had pro-morphogenic properties in a PTEN-deficient Caco-2 model. Fundamental attributes of the model, namely, links between apical aPKC activity readout and gland morphology, were conserved and had prognostic significance in CRC.

## Materials and Methods

### *Reagents and Antibodies*

All laboratory chemicals were purchased from Sigma-Aldrich (Dorset, United Kingdom) unless otherwise stated. The antibodies used in this study were mouse anti-PTEN (Cell Signaling Technology, Danvers, MA); mouse anti-cdc42 and mouse anti–E-cadherin (BD Biosciences, Oxford, United Kingdom); mouse anti–$Na^+/H^+$ exchanger regulatory factor-1 (NHERF-1; LifeSpan Biosciences, Seattle, WA); rabbit anti-aPKCζ (ab51157), rabbit anti–phospho-aPKC (p-aPKC; $Thr^{560}$; ab62372), and rabbit anti–glyceraldehyde phosphate dehydrogenase (GADPH; ab9485; Abcam, Cambridge, MA); rabbit anti-hemagglutinin (HA) and anti–green fluorescent protein (GFP; New England Biolabs, Hitchin, United Kingdom). These primary antibodies were used where appropriate in conjunction with Alexa Fluor 568 (anti-rabbit) and Alexa Fluor 488 (anti-mouse; Molecular Probes, Invitrogen, Carlsbad, CA) and/or anti-mouse cyanine 5 (Jackson ImmunoResearch, Newmarket, United Kingdom) for confocal microscopy.

### *Cell Lines*

PTEN-wt and PTEN-deficient polarizing Caco-2 and Caco-2 ShPTEN colorectal cells [7] were used (see Cell Transfections section below). A PTEN-null subclone of HCT116 cells ($PTEN^{-/-}$ HCT116 cells) [24] was also used for signaling experiments. Caco-2 clones were cultured in minimal essential Eagle's medium supplemented 10% fetal calf serum, 1 mM non-essential amino acids, and 1 mM L-glutamine at 37°C in 5% $CO_2$. $PTEN^{-/-}$ HCT116 cells were cultured in McCoys 5A media supplemented with 10% fetal calf serum, 1 mM L-glutamine, and 1 mM sodium pyruvate.

### *Cell Transfections*

Stable PTEN-deficient Caco-2 ShPTEN cells were generated by transfection of parental Caco-2 cells with replication-defective retroviral vectors encoding PTEN short hairpin RNA (shRNA), using the Phoenix Retroviral Expression System (Orbigen, San Diego, CA) [25] as we have previously described [7,26]. Briefly, Phoenix Eco retroviral packaging cells (Orbigen) were transfected with pMKO.1 puro PTEN shRNA or pMKO.1 puro empty vector (EV) retroviral expression vectors (Addgene, Cambridge, MA), and the supernatant containing recombinant retroviral vectors encoding PTEN shRNA or EV only was collected after 48 hours. Viral supernatant was centrifuged at 2000 rpm and then added to Caco-2 cultures for 48 hours at 37°C in 5% $CO_2$. Caco-2 transfectants were then incubated in 1 μg/ml puromycin for 7 days for selection of ShPTEN or EV-only positive subclones [7,26].

Transient or stable transfections with wt or mutant PTEN constructs were carried out using GeneJuice Transfection Reagent, as we previously described [7,26]. $PTEN^{-/-}$ HCT116 PTEN cells were transiently transfected with wt PTEN or catalytically active or inactive mutants. In Caco-2 ShPTEN cells, many constructs would be repressed by the stably expressed PTEN shRNA that targets a 58-bp region within the PTEN phosphatase coding region [25]. For this reason, PTEN constructs containing a wt or mutant phosphatase domain were not used in these cells. Caco-2 ShPTEN cells were stably transfected with EV only, the isolated PTEN C2 domain (C2), or a C2 domain construct mutated at the calcium binding region 3 membrane-binding loop (C2 M-CBR3) in pEGFP expression vectors. In transient transfections, cells were lysed after 48 hours and cell lysates were probed as described in Protein Extraction and Western

Blot Analysis section. Stable Caco-2 ShPTEN subclones expressing EV, C2, or C2 M-CBR3 were selected in 500 μg/ml G418 and then used in further experiments.

### *Cell Treatment*

Colorectal cells were treated with an aPKC pseudosubstrate inhibitor (PSI) peptide containing a membrane-targeting myristoylation tag that functions as an effective aPKC inhibitor (aPKC-PSI) [27]. aPKC-PSI treatment may induce rapid apoptosis in various cell types at concentrations between 16 and 50 μM [19,28,29]. In this study, the minimal aPKC-PSI concentration that suppressed p-aPKC was determined on initial dose-range studies. Caco-2 cells in 3D culture were then continuously exposed to this minimum aPKC-PSI dose. Effects were assessed on AM p-aPKC, AM NHERF-1 signal intensity and 3D morphogenesis. Caco-2 cells were also treated with sodium butyrate (NaBt), a short-chain fatty acid that upregulates PTEN expression [26,30,31] and PTEN-dependent cdc42 activity [26]. In separate experiments, cells were treated with 1 mM NaBt *versus* vehicle only (VO) control for 48 hours for Western blots or glutathione *S*-transferase (GST) pull-down assays or every 48 hours for 12 days in morphogenesis experiments.

### *Cell Fractionation*

Experiments were conducted as we have previously described [7]. Briefly, cultured cells were isolated in lysis buffer containing protease inhibitors, sonicated, and centrifuged, and the supernatant was retained as the cytosolic fraction. The pellets were resuspended in buffer with 1% Triton X-100 and 0.1% sodium dodecyl sulfate and incubated for 1 hour at 4°C. Membrane fractions were obtained by centrifugation, and the insoluble pellets were discarded [7]. In separate experiments, protein extraction, Western blot analysis, and pull-down assays were conducted in isolated cell membrane and cytosolic fractions.

### *Protein Extraction and Western Blot Analysis*

As previously described [7], proteins were resolved using gel electrophoresis, followed by Western blot analysis onto nitrocellulose membranes. Membranes were probed using antibodies as indicated in the text. Experiments were repeated in triplicate.

### *Cdc42 GST–p21-Activated Kinase Pull-Down Assays*

Cdc42 activity was assayed by GST–p21-activated kinase pull-down assay as previously described [7,26]. Briefly, cells were grown on 90-mm dishes and lysed with 50 mM Tris-HCl (pH 7.5), 1% Triton X-100, 100 mM NaCl, 10 mM $MgCl_2$, 5% glycerol, 1 mM $Na_3VO_4$, and protease inhibitors (Roche Diagnostics, West Sussex, United Kingdom). Lysates were centrifuged at 12,500*g* for 10 minutes. GST–p21-activated kinase fusion protein coupled with Glutathione Sepharose 4B beads (GE Healthcare, Nottingham, United Kingdom) was added to 1 mg of cell lysate. The beads were centrifuged after 1 hour, washed three times, and resuspended in Laemmli buffer with 1 mM DTT. GTP-bound cdc42 was assayed by Western blot analysis.

### *Three-Dimensional Morphogenesis Assays*

Caco-2 and Caco-2 ShPTEN cells were cultured and embedded in Matrigel (BD Biosciences) matrix, as previously described [7]. Briefly, $6 \times 10^4$ trypsinized cells were mixed with Hepes (20 mM) and Matrigel in a final volume of 100 μl, which was plated onto each well of an eight-well chamber slide (Millipore, Watford, United Kingdom), allowed to solidify for 30 minutes at 37°C, and subsequently overlaid with 400 μl of media per well. Cells were cultured and harvested for imaging of 3D morphology by confocal and/or bright-field fluorescence microscopy (FM). Confocal microscopy was conducted at sequential intervals of 2, 4, and 12 days.

### *Confocal Microscopy*

Embedded 3D glandular cultures were fixed in 4% paraformaldehyde for 20 minutes and processed for immunofluorescence, as previously described [7]. Briefly, glands were permeabilized with 0.5% Triton X-100, rinsed, and blocked in buffer containing 0.1% BSA and 5% goat serum. Glands were incubated overnight in primary antibodies against E-cadherin as a basolateral membrane marker and aPKCζ as an AM marker. p-aPKC ($Thr^{560}$) immunofluorescence was used as a marker of aPKC activity [32]. Glands were also incubated in primary antibodies against NHERF-1. Apical NHERF-1 signal intensity was then assessed against that of p-aPKC. The preparations were washed with immunofluorescence buffer (three times, 20 minutes each) and incubated with anti-mouse and/or anti-rabbit Alexa Fluor antibodies. DNA was stained with 4′,6-diamino-2-phenylindole (DAPI) and

**Figure 1.** PTEN functional domains and cdc42 activation. (A) PTEN constructs. Details of wt PTEN and mutant constructs are provided in the text. (B) Effects of PTEN constructs on cdc42 activation in $PTEN^{-/-}$ HCT116 cells. $PTEN^{-/-}$ HCT116 cells were transfected with HA-tagged wt or mutant PTEN constructs. Data are shown in two panels, each containing wt PTEN and EV, placed side by side. Differential gel migration according to size of deletion constructs is shown in the left HA-tagged protein blot. Those constructs containing a C2 domain with intact CBR3 loop (PTEN-wt, PTEN C124S, PTEN G129E, PTEN 1-353, PTEN 175-403) enhanced cdc42 activity more than EV or the PTEN M-CBR3 mutant. (C) Effects of PTEN C2 domain constructs on cdc42 activation in $PTEN^{-/-}$ HCT116 and Caco-2 ShPTEN cells. $PTEN^{-/-}$ HCT116 cells or Caco-2 ShPTEN cells were transfected with a GFP-tagged, isolated wt C2 domain or a C2 domain construct mutated at the CBR3 membrane-targeting loop (C2 M-CBR3) *versus* EV. Detection of GFP tags using specific antibodies is shown. The wt C2 domain (C2) enhanced cdc42 activity more than C2 M-CBR3 or EV, in $PTEN^{-/-}$ HCT116 cells and Caco-2 ShPTEN cells. (D) Subcellular localization of PTEN C2 domain constructs. Expression of GFP-labeled C2, C2 M-CBR3, and EV is shown in cytosol or membrane fractions of Caco-2 ShPTEN cells, identified using anti-GFP antibody. Expressions of the cytosolic marker tubulin and membrane marker E-cadherin are shown (left panel). C2 *versus* C2 M-CBR3 expression in total cell lysate is shown to indicate transfection efficiency. Differential gel migration according to size is shown for GFP-C2 and GFP-EV (right panel). (E) Subcellular localization of PTEN C2 domain constructs. Arbitrary densitometry values in Caco-2 ShPTEN cells transfected with GFP-labeled C2 (left two columns) or C2 M-CBR3 (right two columns). Values for accumulation in cytosol and in membrane fractions for C2 *versus* C2 M-CBR3 were 137 ± 8.5 *versus* 236 ± 8.7 (cytosol) and 221 ± 4.8 *versus* 122 ± 7.2 (membrane) [arbitrary densitometry units; $P < .001$; two-way ANOVA].

chamber slides were mounted using VECTASHIELD Mounting Medium (Vector Scientific, Belfast, United Kingdom). Sequential three-color scan images were taken at gland midsections at room temperature using a Leica SP5 confocal microscope on an HCX PL APO lambda blue 63× 1.40 oil immersion objective at 1× or 2× zoom. Images were collected, processed, and merged, and scale bars were added using LAS AF Leica Confocal Imaging Software (Leica, Wetzlar, Germany). In studies of Caco-2 ShPTEN glands transfected with PTEN C2 domain

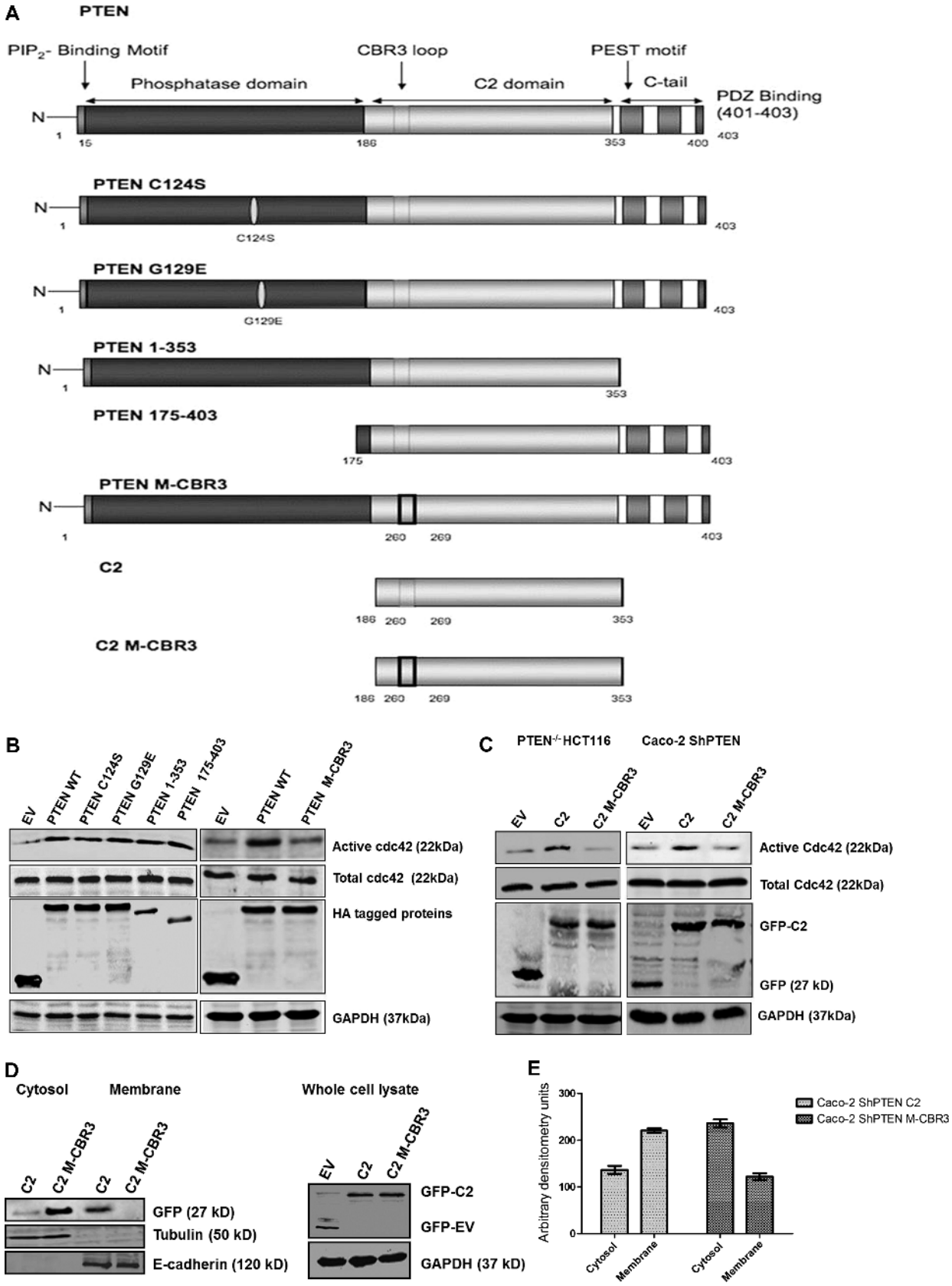

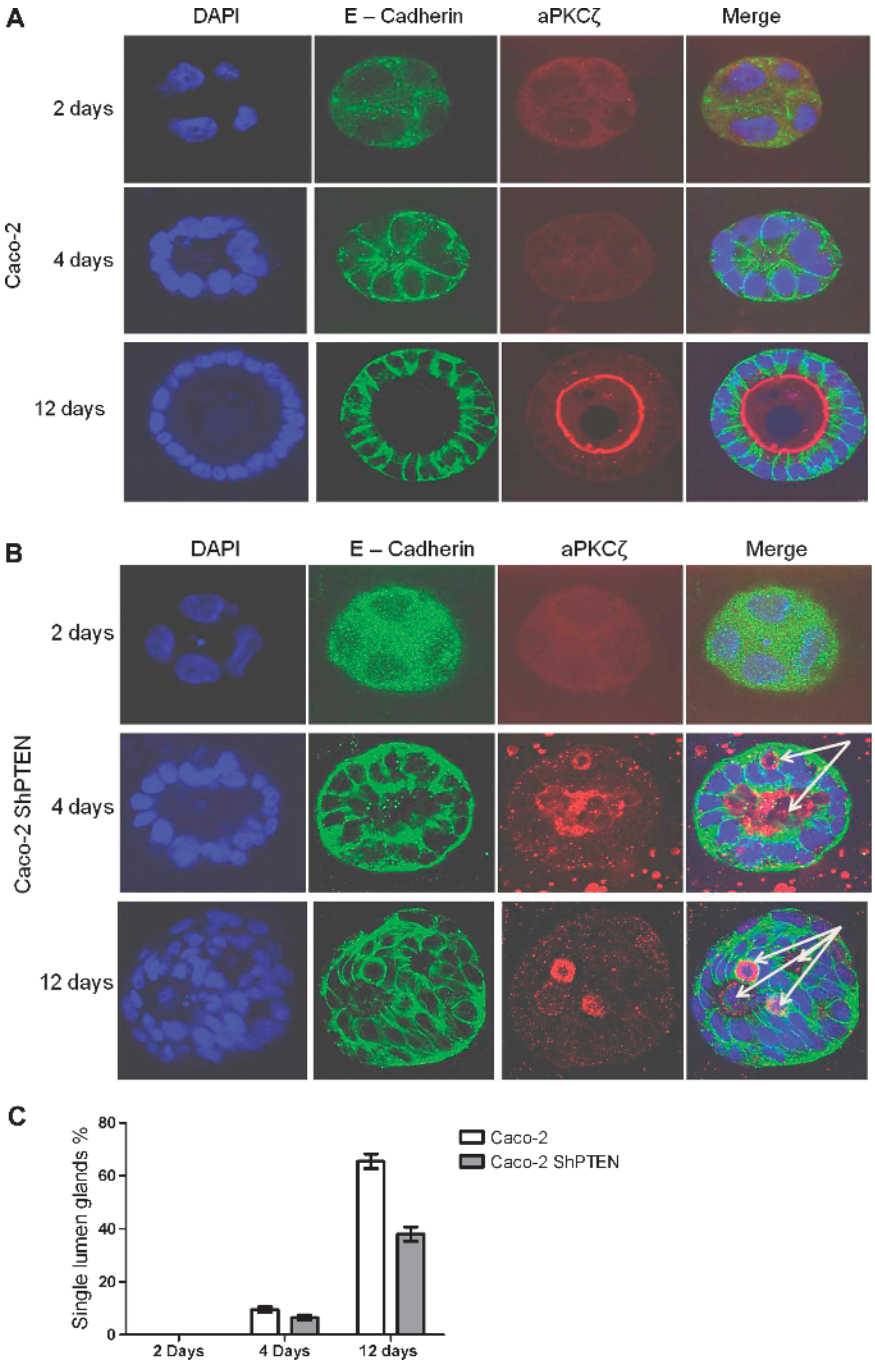


**Figure 2.** Caco-2 and Caco-2 ShPTEN glandular morphogenesis. (A) Progressive Caco-2 glandular morphogenesis. Nuclei were stained in developing glands with DAPI (blue), whereas immunolabeling with anti–E-cadherin (green) and anti-aPKC antibodies was conducted to identify basolateral membrane (green) and AM (red), respectively. Morphology assessments were conducted at 2, 4, and 12 days of culture. A well-formed AM indicated by anti-aPKC immunofluorescence is oriented around single central lumen. (B) Progressive Caco-2 ShPTEN glandular morphogenesis. PTEN-deficient Caco-2 ShPTEN glands showed misorientation of the aPKC AM marker (red) and multiple lumens/vacuoles (arrows) as early as 4 days of culture. (C) Single lumen formation during progressive Caco-2 and Caco-2 ShPTEN glandular morphogenesis. Summary data of single lumen development in Caco-2 and Caco-2 ShPTEN glands (Caco-2 *vs* Caco-2 ShPTEN after 12 days of culture, 65.5 ± 2.75% *vs* 38 ± 2.68%; $n = 3$; $P < .01$; ANOVA) are shown.

constructs, the fluorescent emission spectrum used for visualizing E-cadherin (secondary antibody label of Alexa Fluor 488) overlapped with that of GFP fluorescence. In these experiments, an anti-mouse cyanine 5 antibody conjugate was used for imaging of E-cadherin, with four-color confocal microscopy. The ImageJ toolkit (National Institutes of Health, Bethesda, MD) was used to measure apical signal intensity of p-aPKC or NHERF-1 in untreated and aPKC-PSI–treated Caco-2 glands. Total apical domains surrounding gland lumens were captured in rectangular ImageJ selection windows, and fluorescence was quantified, plotted, and statistically analyzed.

### *Histomorphic Assays in Human CRC*

Specimens from 40 non-consecutive patients who underwent surgery for primary CRC at the Royal Victoria Hospital (Belfast, United Kingdom) between 2008 and 2011 were assessed. Samples were selected on the basis of histology reports to provide approximately equal numbers with good, intermediate, and poor differentiation by conventional histologic grading criteria [33]. All histomorphic data from hematoxylin and eosin–stained slides were reviewed, and clinical data were obtained from corresponding reports. Clinicopathologic information included greatest tumor dimension, Dukes and Tumor, Node, Metastasis stage, and the number of regional lymph nodes involved by metastasis.

### *Assessment of Gland Formation in Human CRC*

Archival paraffin-embedded CRC specimens with surrounding normal mucosa were sectioned at 6-μm intervals and hematoxylin and eosin stained. Each sample was evaluated by one pathologist (M.L.)

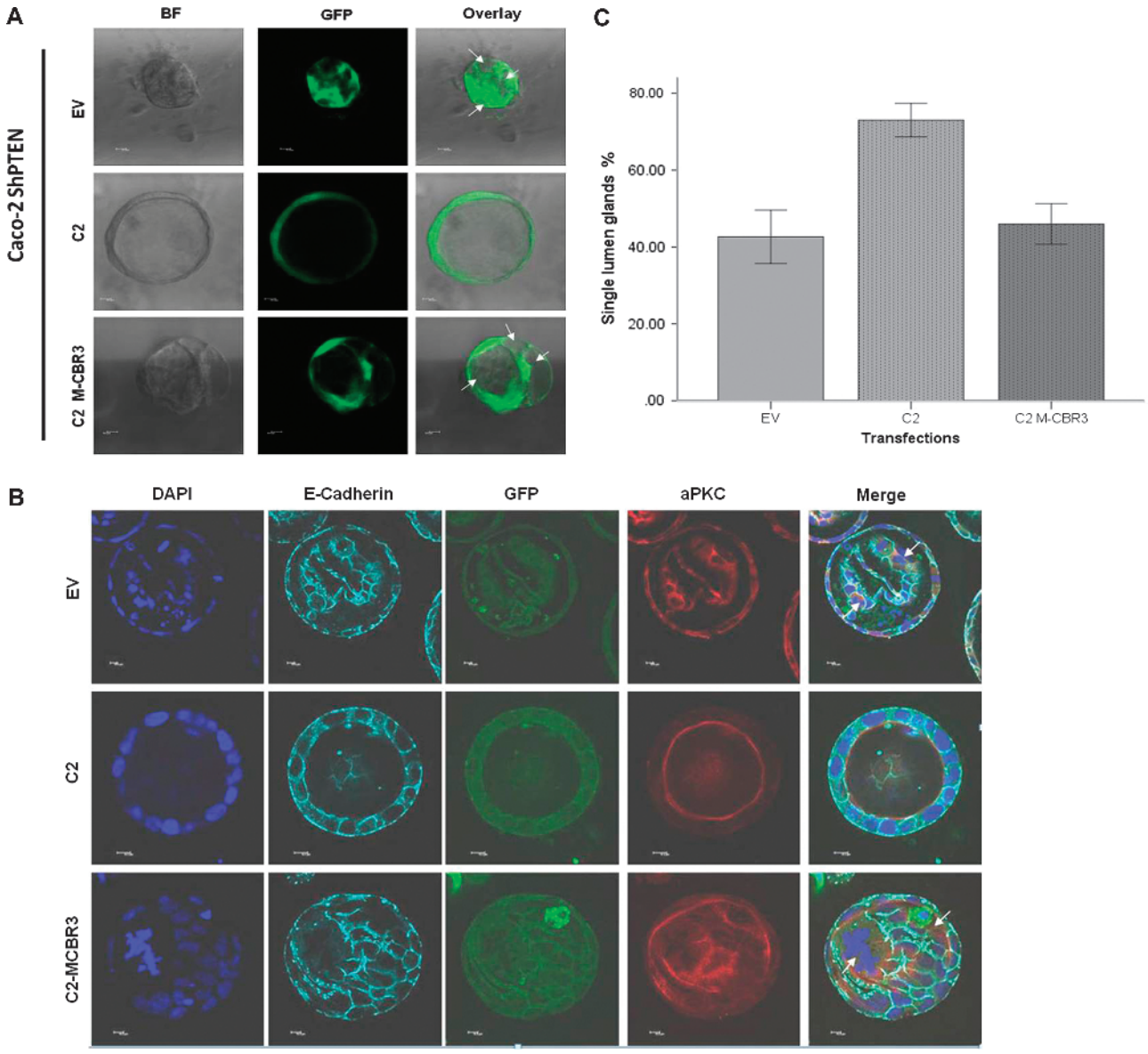


**Figure 3.** Effects of C2 domain transfections on Caco-2 ShPTEN gland morphogenesis. (A) Effects of C2 domain constructs on Caco-2 ShPTEN morphogenesis at 4 days. Stable transfection of Caco-2 ShPTEN cells with C2 (middle row) but not C2 M-CBR3 (bottom row) or EV (top row) rescued single lumen formation during epithelial morphogenesis. Bright-field FM (BF; first column), FM for GFP (green; second column), or overlay (third column) images are shown; 10 × 0.30 dry objective at ×10 magnification. White arrows indicate abnormal lumens. Scale bar, 10 μM. (B) Effects of C2 domain constructs on Caco-2 ShPTEN morphogenesis at 12 days. Caco-2 ShPTEN 3D cultures after stable transfection with GFP-tagged C2 (middle row), C2 M-CBR3 (bottom row), or EV (top row). Confocal midsections of glands imaged for DAPI (blue), E-cadherin (cyan), GFP (green), and aPKC (red) after 12 days of culture. GFP expression (third column) confirms stable transfection with wt or mutant GFP-labeled C2 domain constructs or GFP-labeled EV. White arrows indicate abnormal lumens; 63× 1.40 oil immersion objective at ×2 magnification. Scale bar, 10 μM. (C) Effects of C2 domain transfections on Caco-2 ShPTEN single lumen formation at 12 days. Single lumen formation in Caco-2 ShPTEN glands after transfection (EV *vs* C2 *vs* C2 M-CBR3 = 43.5 ± 4.0% *vs* 73.0 ± 4.4% *vs* 46.0 ± 5.3%; $P = .022$; ANOVA; $n = 3$).

for gland formation according to the method described by Ueno et al. [5]. Briefly, a CRC region in which gland formation is totally absent is defined as the poorly organized region (POR). Grade III is applied to tumors for which the POR fully occupies the microscopic field of a ×40 objective lens. For tumors with a smaller POR, clusters of greater than or equal to five cancer cells without a gland structure were counted in the microscopic field of a ×4 objective lens, in a region where clusters were observed most intensively. Tumors with ≥10 clusters

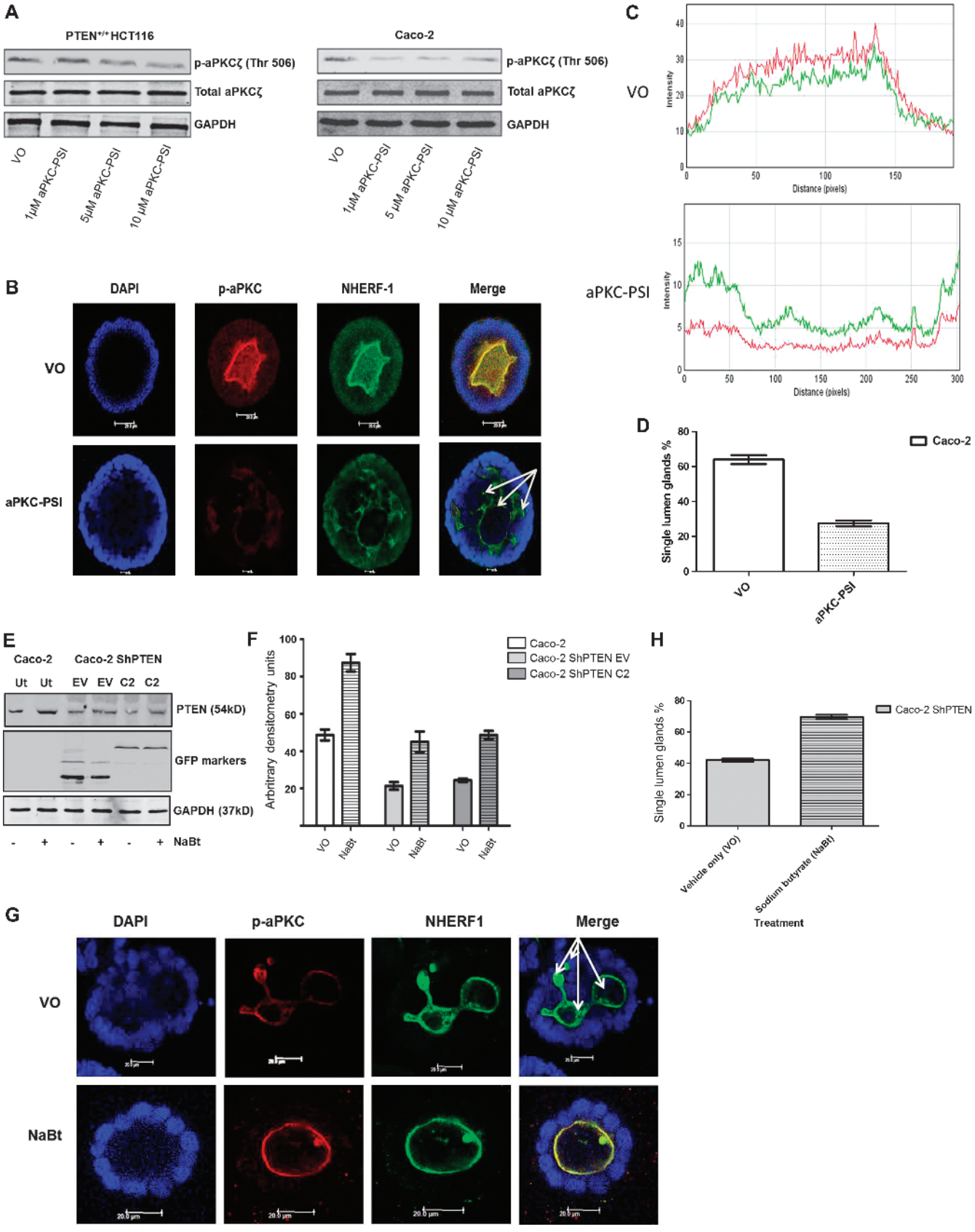

were classified as grade II and those with <10 clusters as grade I [5]. These grades have previously been shown to relate to CRC-specific and overall survival [5].

### *aPKC and NHERF-1 Immunohistochemistry*

Colonic tissue specimens were deparaffinized and hydrated as previously described [34], followed by antigen retrieval in a citrate buffer at pH 6.3 and microwaved at 850 W for 20 minutes. The sections were cooled in running water for 5 minutes, rinsed three times with Tris/HCl-buffered saline (TBS) for 5 minutes, and blocked from nonspecific endogenous peroxide staining by incubation in 3% $H_2O_2$ in methylated spirits for 10 minutes. The anti-aPKCζ and anti–p-aPKCζ antibodies (Abcam) were applied at dilutions between 1:50 and 1:200 in TBS, whereas the NHERF-1 antibody (LifeSpan Biosciences; LS-B1873) was applied at 1:200 in TBS. Antibodies were applied overnight at 4°C, and unbound antibody was removed by washing twice in TBS for 5 minutes. Detection of primary antibody binding was achieved using DAKO EnVision dual link anti-mouse and anti-rabbit detection kit, according to manufacturer's instructions. Sections were counterstained with Mayer's hemalum to show nuclear details and then dehydrated, cleared, and mounted in synthetic mounting medium.

### *Assessment of aPKC or NHERF-1 Membrane Localization in Normal Colon and CRC*

Apical localization of aPKC, p-aPKC, and NHERF-1 was assessed in tissue sections of normal colon and CRC. Initial studies involved aPKC or p-aPKC immunohistochemistry. NHERF-1 AM localization in CRC has been shown previously [35]. In this study, assessment of NHERF-1 staining intensity was carried out in apical regions of columnar epithelium of normal colon and at the centers of lumen-like structures in CRCs. Tissue sections were then scored for AM staining intensity on a graded scale from 0 to 3. Scoring was conducted over 40 low power fields (×10 magnification) per tumor by two independent assessors (R.T. and J.E.) who were unfamiliar with tumor grading methodology and blinded to tumor grade. The highest intensity of staining present in each field and the percentage of the field exhibiting this intensity of staining were estimated within 20% increments. The final score for each field was taken as the product of these assessments. Consensus scores were estimated on completion.

### *Data Analysis*

Descriptive statistics were expressed as the means ± SEM. Statistical analysis of subcellular localization of PTEN C2 or C2 M-CBR3 constructs was performed by two-way analysis of variance (ANOVA). Analysis of transfection or treatment effects on 3D glandular morphogenesis was performed by one- or two-way ANOVA or Student's *t* test. Pearson test was used to assess correlation between p-aPKC and NHERF-1 signal intensities at the AM. To assess NHERF-1 AM intensity (AMI) against categorical covariates of CRC histologic grades, NHERF-1 data were log transformed and tested by a hierarchical (nested) ANOVA analysis [36]. Correlations between NHERF-1 AMI and lymph node involvement were investigated by Kendall $\tau$ test. SPSS for Windows release 20.0 (IBM Corp, New York, NY) and GraphPad Prism V5 for Windows (GraphPad Software, La Jolla, CA) statistical software packages were used.

## Results

### *Effects of Catalytically Active or Inactive PTEN Constructs on cdc42 Activity*

$PTEN^{-/-}$ HCT116 cells were transfected with wt PTEN or one of a panel of mutant, deletion, or truncation constructs, including PTEN C124S and G129E that lack lipid and protein phosphatase or lipid phosphatase activity, respectively, PTEN 1-353 (lacking the C-terminal tail), the phosphatase domain deletion PTEN 175-403, PTEN M-CBR3 bearing the C2 domain CBR3 mutation at residues 263 to 269, the isolated C2 domain (residues186-353), and the isolated C2 domain bearing the CBR3 mutation (C2 M-CBR3) [37], in expression vectors (Figure 1*A*). Isolated phosphatase domains

**Figure 4.** NHERF-1 as readout of apical aPKC activity. (A) Effects of aPKC-PSI treatment on p-aPKC in colorectal cells. Limited dose-response assay of aPKC-PSI treatment *versus* p-aPKC in colorectal cells. In Caco-2 cells, 1 μM aPKC-PSI suppressed p-aPKC. (B) Effects of aPKC-PSI treatment on apical p-aPKC, NHERF-1, and Caco-2 gland morphogenesis. VO-treated Caco-2 glands predominantly formed single central lumens with high apical aPKCζ activity (indicated by p-aPKCζ) and NHERF-1 signal intensity. Treatment with a myristoylated aPKC peptide inhibitor suppressed apical aPKCζ activity (p-aPKCζ; T560) and apical NHERF-1 signal intensity and induced a multilumen phenotype (multiple lumens indicated by white arrows). Scale bar, 10 μM. (C) Effects of aPKC-PSI treatment on p-aPKC and NHERF-1 apical signal intensities. p-aPKC (red) and NHERF-1 (green) signal intensities were assessed in apical domains surrounding the whole circumference of the central lumens of Caco-2 glands treated by VO (DMSO; top panel) or a myristoylated aPKC peptide inhibitor (aPKC-PSI; bottom panel; $n = 20$ per treatment group). Signal intensities (mean ± SEM) are given as follows: VO–p-aPKC—21.2 ± 0.9; NHERF-1—12.1 ± 0.6; *versus* aPKC-PSI–p-aPKC—4.6 ± 0.24; NHERF-1—5.7 ± 0.28). Apical p-aPKC and NHERF-1 signal intensities correlated after VO and aPKC-PSI treatments (Pearson correlation = 0.86; $P < .001$). (D) Effects of aPKC-PSI treatment on Caco-2 gland lumen formation. Single central lumens formed in 64 ± 2.6% Caco-2 glands treated with VO *versus* 27.5 ± 1.7% (VO) treated with aPKC-PSI ($P < .001$; one-way ANOVA). (E) Effects of NaBt treatment on PTEN expression. Treatment of Caco-2 or Caco-2 ShPTEN cells with NaBt (1 mM) increased PTEN protein expression in untransfected (Ut) Caco-2 cells and in Caco-2 ShPTEN cells after EV transfection (EV) or transfection with the isolated PTEN C2 domain (C2) in expression vectors. (F) Summary effects of NaBt treatment on PTEN protein expression. NaBt treatment enhanced PTEN protein expression in Caco-2 cells *versus* VO (87.3 ± 4.7 *vs* 48.7 ± 2.9 arbitrary densitometry units) and in Caco-2 ShPTEN cells after EV (45.0 ± 5.5 *vs* 21.3 ± 2.0) or C2 transfections (48.7 ± 21 *vs* 24.3 ± 0.9; $P < .001$; two-way ANOVA; $n = 3$). (G) Effects of NaBt treatment on Caco-2 ShPTEN gland morphogenesis. NaBt treatment (bottom panel) enhanced single lumen formation in excess of VO (top panel) in Caco-2 ShPTEN glands. AMs in single and multilumen (white arrows) glands were identified by aPKC and NHERF-1 immunofluorescence. Scale bar, 20 μM. (H) NaBt treatment effects on single lumen formation in Caco-2 ShPTEN glands. Summary effects of NaBt treatment on Caco-2 ShPTEN glandular morphogenesis (percentage of single lumen glands after 12 days of culture; Caco-2 ShPTEN VO = 42.0 ± 1.0 *vs* NaBt = 69.5 ± 1.5; $P < .01$; Student's *t* test).

(residues 1-185), isolated C-terminal regions (353-403), and PTEN mutants that lack the C2 domain are unstable with low protein stability [38] and were not investigated. Transfection of PTEN$^{-/-}$ HCT116 cells with wt PTEN, G129E, C124S, PTEN 175-403, and PTEN 1-353 enhanced cdc42 activation, in excess of EV-transfected controls. Conversely, PTEN M-CBR3 transfection did not upregulate cdc42 activity (Figure 1*B*). Transfection of PTEN$^{-/-}$ HCT116 or Caco-2 ShPTEN cells with the isolated C2 domain enhanced cdc42 activity, whereas C2 M-CBR3 transfection had no demonstrable effect (Figure 1*C*). Hence, PTEN constructs with an intact C2 domain enhanced cdc42 activity in PTEN$^{-/-}$ HCT116 and Caco-2 ShPTEN cells. Because PTEN colocalization with cdc42 at the AM is implicated in cell polarization and 3D morphogenesis [17], we investigated membrane localization of the PTEN C2 domain constructs in GFP-containing expression vectors by transfection, cell fractionation, and immunoblot experiments in Caco-2 ShPTEN cells. The intact PTEN C2 domain showed greater membrane localization than C2 M-CBR3 or EV, whereas the C2 M-CBR3 construct was localized in the cytosol (Figure 1, *D* and *E*).

### *Effects of PTEN on Stepwise 3D Glandular Morphogenesis*

Although PTEN activates cdc42 [17] and is required for effective 3D epithelial morphogenesis [7,17], effects of PTEN on early Caco-2 morphogenesis stages were unclear. To investigate this theme, Caco-2 and Caco-2 ShPTEN cells were grown in 40% Matrigel, fixed, and immunostained for E-cadherin (basolateral marker) and aPKC (apical marker), whereas nuclear DNA was stained with DAPI at 2, 4, and 12 days of culture. Progressive glandular morphogenesis was assessed by confocal microscopy. By 2 days, cells formed distinct aggregates, whereas lumen formation was discernible in a minority of Caco-2 and Caco-2 ShPTEN cultures by 4 days. Between 4 and 12 days, greater differences in glandular morphogenesis were observed. As Caco-2 cells proliferated and glands enlarged, the AM identified by the aPKC marker was localized at gland centers as a uniform continuous interface with a single central lumen until development of mature glands by 12 days (Figure 2*A*). Whereas single lumens also developed in some Caco-2 ShPTEN glands between 4 and 12 days, the majority showed gross mispositioning of the aPKC AM marker and development of multiple lumens or vacuoles. These changes were detectable as early as 4 days until maturity of dysmorphic Caco-2 ShPTEN glands at 12 days (Figure 2, *B* and *C*).

### *Effects of the PTEN C2 Domain Constructs on 3D Glandular Morphogenesis*

Because cdc42 could be activated in PTEN-deficient cells by transfection of an isolated C2 domain but not by C2 M-CBR3, we investigated effects of those constructs on 3D glandular morphogenesis. Caco-2 ShPTEN cells were stably transfected with the intact PTEN C2 domain, EV, or C2 M-CBR3 in EGFP expression vectors. Glands were processed and imaged by bright-field FM or for GFP using specific antibodies and FM at 4 days and for aPKC, DAPI, E-cadherin, and GFP using specific antibodies and confocal microscopy at 12 days of culture. Transfection of Caco-2 ShPTEN cells with the intact PTEN C2 domain rescued glandular morphogenesis, leading to formation of a single central lumen. Conversely, the C2 M-CBR3 construct was ineffective and was associated with a multilumen phenotype, comparable to EV-transfected Caco-2 ShPTEN glands (Figure 3, *A*–*C*). No differences of AM localization of GFP-labeled C2 or C2 M-CBR3 were shown in 3D Caco-2 ShPTEN cultures. In summary, we found that the isolated PTEN C2 domain but not C2 M-CBR3 rescues Caco-2 ShPTEN glandular morphogenesis.

### *Apical p-aPKC and NHERF-1 in 3D Colorectal Gland Models*

p-aPKC is indicative of aPKC activity [32] and was suppressed in Caco-2 cultures by aPKC-PSI treatment, at concentrations between 1 and 10 μM (Figure 4*A*). Caco-2 cells were then incubated in DMSO VO or aPKC-PSI (1 μM) for 12 days in morphogenesis studies. p-aPKC colocalized with NHERF-1 at apical domains of VO-treated Caco-2 glands (Figure 4*B*). aPKC-PSI treatment suppressed p-aPKC and NHERF-1 AM signal intensities and perturbed morphogenesis leading to a multilumen phenotype in Caco-2 glands (Figure 4, *B* and *C*). Apical signal intensities of p-aPKC and NHERF-1 correlated in untreated and aPKC-PSI–treated Caco-2 glands (Figure 4*D*), indicating that NHERF-1 may provide readout of apical aPKC pro-morphogenic activity. To further investigate the use of NHERF-1 as an AM marker, we conducted experiments aimed at rescue of defective Caco-2 ShPTEN morphogenesis. NaBt can enhance PTEN expression and PTEN-dependent cdc42 activity in Caco-2 ShPTEN cells [26]. Furthermore, up-regulation of PTEN by targeted treatment can rescue Caco-2 ShPTEN morphogenesis [7]. In the present study, NaBt treatment enhanced PTEN protein expression in Caco-2 and Caco-2 ShPTEN wt cells and/or after EV or C2 transfections (Figure 4, *E* and *F*). NaBt treatment also rescued single lumen formation in Caco-2 ShPTEN glands (Figure 4*G*). NHERF-1 colocalized with aPKC and provided a suitable AM marker in these experiments (Figure 4, *G* and *H*). Caco-2 ShPTEN glands were smaller after NaBt than VO treatment (Figure 4*G*).

### *Grading of Gland Morphology of Human CRC*

Because NHERF-1 provided a useful AM marker and correlated with apical p-aPKC, NHERF-1 AMI was assessed against gland morphology and prognostic variables in 40 human CRCs. Maximum tumor diameter in colectomy specimens ranged from 15 to 100 (mean ± SEM = 44.2 ± 3.32) mm. Five CRCs were Dukes stage A, 16 Dukes B, and 19 Dukes C. A mean of 14 lymph nodes was retrieved with colectomy specimens (10-41), and a mean of 2.3 (0-17) lymph nodes was involved in tumor metastasis. None of the CRCs was associated with clinically detectable distant metastases at the time of colectomy. CRCs were recategorized in three grades according to previously defined criteria for assessment of gland morphology [5]. Twenty-four had a POR lacking gland formation that fully occupied a field visualized through a ×40 objective lens and were categorized as grade III. The remainder has smaller PORs, of whom 9 had $\geq$10 clusters of $\geq$5 cancer cells without gland morphology seen through a ×4 objective lens and 7 had <10 such clusters, categorized as grades II and I, respectively (Figure 5, *A*–*C*).

### *Assessment of AM NHERF-1 Expression against Gland Morphology in Human CRCs*

NHERF-1 enrichment at the epithelial apical domain was shown in normal colon (Figure 6*A*). Conversely, aPKC and p-aPKC were expressed but not apically localized in normal colon, making these markers unsuitable for further translational studies (data not shown). NHERF-1 apical intensity was graded 0 to 3 in normal mucosa at least 5.0 cm distant from tumors and in CRCs, across 40 fields per section, by two independent observers. NHERF-1 apical intensity scores were

greater in normal mucosa (1.55 ± 0.03; Figure 6*A*) than in CRCs of all grades (grade I, 0.32 ± 0.02 to grade III, 0.127 ± 0.03; $P < .001$; ANOVA; Figure 6, *B*–*E*). In CRCs, NHERF-1 AMI correlated inversely with CRC grade (Figure 6*F*) and regional lymph node metastases (Figure 6*G*).

## Discussion

We and others have previously shown that PTEN regulates cdc42-dependent 3D glandular morphogenesis [7,17]. In this report, we investigated PTEN phosphatase–dependent or PTEN phosphatase–independent regulation of gland development and assessed translational relevance of 3D Caco-2 organotypic model systems. Our findings reveal that the PTEN C2 domain has an important pro-morphogenic function in 3D Caco-2 models. Furthermore, associations between AM aPKC activity readout and gland morphology in Caco-2 models [19,23] were preserved and had prognostic significance in CRCs.

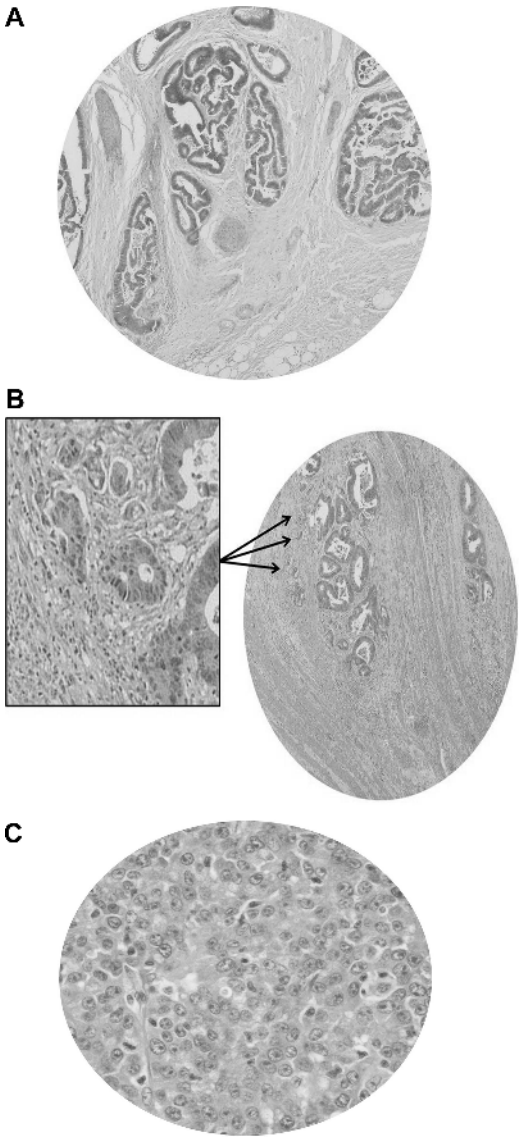


**Figure 5.** Histologic grading of CRC. (A) Grade I CRC. Cancers are made up entirely of irregular glands lined by polarized epithelium oriented around distorted central lumens. (B) Grade II CRC. The primary tumor shows gland formation, but >10 clusters of ≥5 cancer cells lacking a gland-like structure (arrows) are observed, through a ×4 objective lens, in the stroma. A high-power view of some clusters is shown in the framed inset. (C) Grade III CRC. A POR lacking gland morphology fully occupies the field of a ×40 objective lens.

As binding partners of proteins and AM phospholipids, C2 domains may be implicated in translocation of key molecules to membrane subregions [39]. The intact PTEN C2 domain is biologically active, influences polarized growth, suppresses directional migration in cell monolayers [40], and inhibits morphogenic growth of embryonic primitive streak mesenchyme as effectively as wt PTEN [41]. Isolated C2 domains of other lipid-metabolizing enzymes lack these biologic properties. For example, C2 domains of synaptotagmin-like proteins are structurally similar to PTEN C2 [37] but do not suppress directional cell migration [40]. Furthermore, the presence of intact C2 domains in synaptotagmin-like protein mutants promotes AM localization but do not influence 3D morphogenesis of Madin Darby caninine kidney (MDCK) cells epithelial cyst–like structures [42]. In the present study, we found that PTEN mutants containing or comprising an intact C2 domain enhanced cdc42 activity in excess of EV control in transfection studies of $PTEN^{-/-}$ HCT116 or Caco-2 ShPTEN cells. Conversely, transfection of membrane-targeting domain mutants of the CBR3 loop within the C2 domain in full-length PTEN (PTEN M-CBR3) or within the isolated C2 domain (C2 M-CBR3) [37] had no demonstrable effects on cdc42 activity. In subcellular localization studies, we found that transfected C2 constructs accumulated in cell membrane fractions, whereas the C2 M-CBR3 mutant was predominantly retained in cytosol.

A previous study showed that PTEN activation of cdc42 may be linked to lipid phosphatase–dependent enrichment of phosphatidylinositol 4,5-bisphosphate at AMs [17]. This event attracts annexin 2, a membrane-binding protein [43] that binds cdc42 at the AM. By this mechanism, cdc42 is recruited to AM regions in proximity to juxtamembrane guanine nucleotide exchange factors, leading to cdc42 activation and morphogenic growth [17]. However, multiple mechanisms can promote cdc42 membrane clustering, including cytoskeleton-mediated targeting [44], scaffolding proteins [45], specific guanine nucleotide exchange factors [46], and membrane phospholipid movements [47], suggesting some context-specific redundancy of these processes. The isolated PTEN C2 domain binds the universal scaffold protein β-arrestin with greater affinity than full-length PTEN [48]. β-Arrestins act as platforms for orchestration of cytoskeletal processes [49] and inhibit ARHGAP21 [50], a cdc42 GTPase activating protein [51,52]. Hence, PTEN C2 could activate cdc42 for AM assembly and glandular morphogenesis by promoting juxtamembrane accumulation of β-arrestin and suppression of ARHGAP21. Further work beyond the scope of this manuscript is required to investigate this concept.

Whereas PTEN modulates cdc42 signaling [7,17,26] and transfection of PTEN-deficient Caco-2 ShPTEN cells with cdc42 effectively rescues gland morphology [7], PTEN effects on early Caco-2 glandular morphogenesis were unclear. In the present study, we found that PTEN knockdown was associated with impairment of AM integrity and AM mislocalization from early stages of Caco-2 glandular morphogenesis, and multiple abnormal lumens or ectopic vacuoles were detected as early as 4 days of culture. These changes recapitulate effects of cdc42 knockdown [6] and support the role of cdc42 as an essential PTEN-dependent effector of early morphogenesis in this colorectal model. Dissection of PTEN/cdc42 pro-morphogenic signaling could thus identify therapeutic targets that may help arrest colorectal tumor progression early in its course.

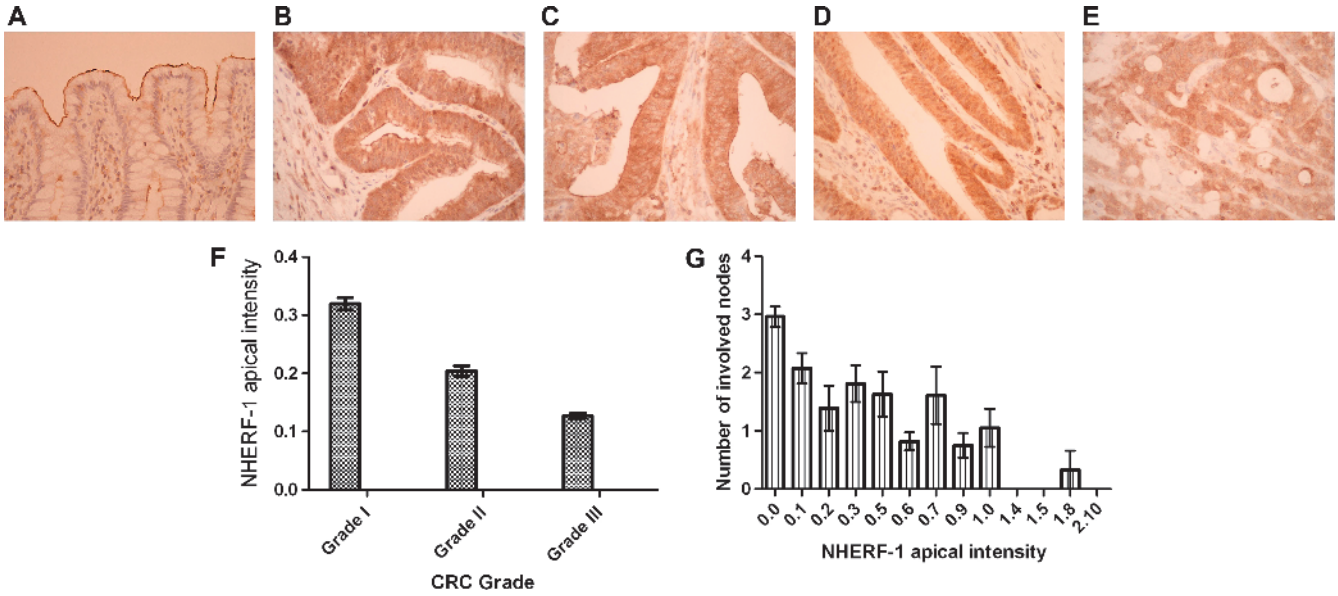


**Figure 6.** NHERF-1 apical localization in human colon. (A) NHERF-1 apical localization in normal colon. AM localization of NHERF-1 in normal human colon (original magnification, ×40). NHERF-1 apical intensity score (mean ± SEM) = 1.55 ± 0.03. (B) NHERF-1 apical localization in CRC (score 3). (C) NHERF-1 apical localization in CRC (score 2). (D) NHERF-1 apical localization in CRC (score 1). (E) NHERF-1 apical localization in CRC (score 0). (F) NHERF-1 apical intensity *versus* cancer grade. NHERF-1 apical intensity scores are given as follows: grade I CRCs = 0.32 ± 0.06; grade II = 0.204 ± 0.05; grade III = 0.127 ± 0.03 ($P = .02$; log transformation and hierarchical ANOVA; error bars denote SEM. (G) NHERF-1 apical intensity *versus* lymph node metastases. Low NHERF-1 apical expression associates with high numbers of involved nodes (error bars denote SEM; $P < .01$; Kendall $\tau$ test).

Because cdc42 activity in PTEN-deficient cells can be enhanced by transfection of the isolated PTEN C2 domain (C2), we investigated the effects of C2 domain constructs on 3D glandular morphogenesis of PTEN-deficient Caco-2 ShPTEN cultures. We found that stable transfection of Caco-2 ShPTEN cultures with C2 domain but not C2 M-CBR3 rescued glandular morphogenesis and restored single lumen formation. In a previous study, the suppressive effect of the isolated PTEN C2 domain on embryonic development of primitive streak mesenchyme was dependent on the integrity of the CBR3 loop [41]. Taken together, these studies support an important role for the PTEN C2 domain in cdc42 activation and morphogenesis, mediated in part through CBR3-dependent membrane binding.

In contrast to our findings of membrane localization of the isolated C2 domain in cell monolayer fractionation experiments, we did not observe any clear difference of AM localization between GFP-labeled C2 or C2 M-CBR3 constructs in our 3D morphogenesis experiments. However, AM lipid subdomains become compartmentalized to enhance signal transduction efficiency during epithelial morphogenesis and differentiation [53]. Within the AM, lipid rafts (LRs) develop as spatiotemporal signaling platforms by clustering or exclusion of membrane proteins and signaling molecules [54]. Selective recruitment or exclusion of PTEN from AM LR domains may represent a key mechanism for spatiotemporal control of rapid or slow Akt-dependent processes [55]. Membrane microdomain compartmentalization of PTEN can permit rapid Akt-activation of essential ion transport [56] while also enabling more protracted regulation of Akt-dependent differentiation processes [56,57]. Within the AM, PTEN predominantly localizes to LRs in terminally differentiated ileal enterocytes [56]. Conversely, in partially differentiated Caco-2 cells, PTEN is excluded from AM LRs to enable high raft Akt2 activity [56]. Signaling molecules may be recruited to LRs through their C2 domains [58]. In the context of the present study, the partially differentiated status of Caco-2 cells in developing 3D glands may impede PTEN C2 domain recruitment to AM LRs but not from whole-cell membrane fractions isolated from cell monolayers.

Three-dimensional culture systems recapitulate cell membrane and junctional dynamics of normal tissue [59] and are suitable for investigation of oncogenic disruption of glandular architecture. In 3D model systems, cdc42 promotes membrane recruitment and activation of aPKCζ that is indispensable for apical domain development [60] and 3D morphogenesis [19,61]. To assess disease relevance of the 3D Caco-2 models, we investigated apical aPKC readout against gland morphology in 3D Caco-2 models and human CRCs. We found aPKC and p-aPKC expression but not apical enrichment in human tissue sections possibly due to tissue processing, fixation artifact, or antibody specificity limitations. Apical aPKC phosphorylates ezrin [62,63] that enables ezrin–NHERF-1 binding [64] and AM localization of the complex [62]. NHERF-1 is a 50-kDa adaptor molecule that has a key role in organization of epithelial AM proteins [65]. To investigate apical NHERF-1 as a potential readout of AM aPKC activity, we conducted colocalization/expression studies in aPKC-PSI–treated and untreated 3D gland models.

NHERF-1 and p-aPKC colocalized at AMs of VO-treated Caco-2 3D glands, and their signal intensities were correlated. Treatment with aPKC-PSI inhibited p-aPKCζ in Caco-2 cell monolayers, suppressed AM p-aPKCζ and NHERF-1 signal intensities in 3D Caco-2 cultures, and disrupted morphogenesis. Our findings concerning gland development accord with previous studies showing that aPKC-PSI induced mitotic spindle misorientation in MDCK cells [46] and impaired 3D morphogenesis in mammary acini [61], whereas small interfering RNA knockdown of aPKCζ induced a multilumen phenotype in 3D Caco-2 cultures [19]. To further investigate the

use as an AM marker, we then assessed NHERF-1 against aPKC localization in experiments aimed at rescue of dysmorphogenesis of PTEN deficiency. We had previously shown that NaBt upregulates PTEN and PTEN-dependent cdc42 signaling [26] but had not previously tested butyrate against glandular morphogenesis. In the present study, we confirmed our previous findings concerning NaBt up-regulation of PTEN [26] and showed that NaBt treatment successfully restored single lumen formation in Caco-2 ShPTEN glands. In these experiments, NHERF-1 AM localization mirrored that of aPKC. NaBt-treated glands were small in size, possibly as a result of NaBt pro-apoptotic or pro-differentiation properties in Caco-2 and Caco-2 ShPTEN cells [26,66] or other effects mediated by butyrate modification of epigenetic events and gene expression in colorectal epithelium [67].

Using a semiquantitative immunohistochemistry scoring system, we found stronger NHERF-1 AM localization in normal colon than in CRCs, in accord with a previous report [35]. In CRCs, we also found an inverse relationship between AM NHERF-1 expression and histologic grading based on gland morphology. Grade I tumors are characterized by irregular gland lumens, whereas grade III cancers are characterized by loss of gland lumen formation within PORs of tumors [5]. NHERF-1 AM scores were also inversely related to metastatic lymph node invasion. These findings support translational relevance of the model system and suggest that suppression of AM aPKC morphogenic signaling may have a key role in evolution of high-grade cancer.

Collectively, this study shows that the catalytically inert PTEN C2 domain regulates cdc42 activation, AM integrity, and 3D gland formation in a CRC model system with high translational relevance. Functional readout of cdc42-dependent apical aPKC activity associates with gland morphology in model systems and CRC. Hence, molecular dissection of apical domain biogenesis in model systems may identify biosignatures of aggressive high-grade cancer as well as promising targets for therapeutic intervention.

## Acknowledgments

We are greatly indebted to T. Waldman (Georgetown University, Washington DC) for supply of $PTEN^{-/-}$ HCT116 cells and A. Hall (Memorial Sloan-Kettering Cancer Center, New York, NY) for provision of wt PTEN constructs as well as PTEN C124S, PTEN G129E, PTEN 1-353, and PTEN 175-403. We are grateful to N. R. Leslie (Heriot-Watt University, Edinburgh, United Kingdom) for provision of PTEN M-CBR3, the isolated PTEN C2 domain, as well as C2 M-CBR3. The authors gratefully acknowledge S. Church for his assistance with imaging and the Northern Ireland Biobank for access to archival human colorectal tissue samples.

## References

[1] Siegel R, Naishadham D, and Jemal A (2012). Cancer statistics, 2012. *CA Cancer J Clin* **62**, 10–29.

[2] Compton CC, Fielding LP, Burgart LJ, Conley B, Cooper HS, Hamilton SR, Hammond ME, Henson DE, Hutter RV, Nagle RB, et al. (2000). Prognostic factors in colorectal cancer. College of American Pathologists Consensus Statement 1999. *Arch Pathol Lab Med* **124**, 979–994.

[3] Härmä V, Knuuttila M, Virtanen J, Mirtti T, Kohonen P, Kovanen P, Happonen A, Kaewphan S, Ahonen I, Kallioniemi O, et al. (2012). Lysophosphatidic acid and sphingosine-1-phosphate promote morphogenesis and block invasion of prostate cancer cells in three-dimensional organotypic models. *Oncogene* **31**, 2075–2089.

[4] Friedl P and Gilmour D (2009). Collective cell migration in morphogenesis, regeneration and cancer. *Nat Rev Mol Cell Biol* **10**, 445–457.

[5] Ueno H, Mochizuki H, Hashiguchi Y, Ishiguro M, Kajiwara Y, Sato T, Shimazaki H, Hase K, and Talbot IC (2008). Histological grading of colorectal cancer: a simple and objective method. *Ann Surg* **247**, 811–818.

[6] Jaffe AB, Kaji N, Durgan J, and Hall A (2008). Cdc42 controls spindle orientation to position the apical surface during epithelial morphogenesis. *J Cell Biol* **183**, 625–633.

[7] Jagan I, Fatehullah A, Deevi RK, Bingham V, and Campbell FC (2013). Rescue of glandular dysmorphogenesis in PTEN-deficient colorectal cancer epithelium by PPARγ-targeted therapy. *Oncogene* **32**, 1305–1315.

[8] Wallace SW, Durgan J, Jin D, and Hall A (2010). Cdc42 regulates apical junction formation in human bronchial epithelial cells through PAK4 and Par6B. *Mol Biol Cell* **21**, 2996–3006.

[9] Pease JC and Tirnauer JS (2011). Mitotic spindle misorientation in cancer—out of alignment and into the fire. *J Cell Sci* **124**, 1007–1016.

[10] Leung CT and Brugge JS (2012). Outgrowth of single oncogene-expressing cells from suppressive epithelial environments. *Nature* **482**, 410–413.

[11] Nakajima YI, Meyer EJ, Kroesen A, McKinney SA, and Gibson MC (2013). Epithelial junctions maintain tissue architecture by directing planar spindle orientation. *Nature* **500**, 359–362.

[12] Bilder D (2004). Epithelial polarity and proliferation control: links from the Drosophila neoplastic tumor suppressors. *Genes Dev* **18**, 1909–1925.

[13] Bilder D, Li M, and Perrimon N (2000). Cooperative regulation of cell polarity and growth by *Drosophila* tumor suppressors. *Science* **289**, 113–116.

[14] Shao J, Washington MK, Saxena R, and Sheng H (2007). Heterozygous disruption of the *PTEN* promotes intestinal neoplasia in $APC^{min/+}$ mouse: roles of osteopontin. *Carcinogenesis* **28**, 2476–2483.

[15] Sawai H, Yasuda A, Ochi N, Ma J, Matsuo Y, Wakasugi T, Takahashi H, Funahashi H, Sato M, and Takeyama H (2008). Loss of PTEN expression is associated with colorectal cancer liver metastasis and poor patient survival. *BMC Gastroenterol* **8**, 56.

[16] Li XH, Zheng HC, Takahashi H, Masuda S, Yang XH, and Takano Y (2009). PTEN expression and mutation in colorectal carcinomas. *Oncol Rep* **22**, 757–764.

[17] Martin-Belmonte F, Gassama A, Datta A, Yu W, Rescher U, Gerke V, and Mostov K (2007). PTEN-mediated apical segregation of phosphoinositides controls epithelial morphogenesis through Cdc42. *Cell* **128**, 383–397.

[18] Tepass U (2012). The apical polarity protein network in *Drosophila* epithelial cells: regulation of polarity, junctions, morphogenesis, cell growth, and survival. *Annu Rev Cell Dev Biol* **28**, 655–685.

[19] Durgan J, Kaji N, Jin D, and Hall A (2011). Par6B and atypical PKC regulate mitotic spindle orientation during epithelial morphogenesis. *J Biol Chem* **286**, 12461–12474.

[20] Qiu RG, Abo A, and Steven Martin G (2000). A human homolog of the *C. elegans* polarity determinant Par-6 links Rac and Cdc42 to PKCζ signaling and cell transformation. *Curr Biol* **10**, 697–707.

[21] Yamanaka T, Horikoshi Y, Suzuki A, Sugiyama Y, Kitamura K, Maniwa R, Nagai Y, Yamashita A, Hirose T, Ishikawa H, et al. (2001). PAR-6 regulates aPKC activity in a novel way and mediates cell-cell contact-induced formation of the epithelial junctional complex. *Genes Cells* **6**, 721–731.

[22] Song MS, Salmena L, and Pandolfi PP (2012). The functions and regulation of the PTEN tumour suppressor. *Nat Rev Mol Cell Biol* **13**, 283–296.

[23] Magudia K, Lahoz A, and Hall A (2012). K-Ras and B-Raf oncogenes inhibit colon epithelial polarity establishment through up-regulation of c-myc. *J Cell Biol* **198**, 185–194.

[24] Lee C, Kim JS, and Waldman T (2004). *PTEN* gene targeting reveals a radiation-induced size checkpoint in human cancer cells. *Cancer Res* **64**, 6906–6914.

[25] Boehm JS, Hession MT, Bulmer SE, and Hahn WC (2005). Transformation of human and murine fibroblasts without viral oncoproteins. *Mol Cell Biol* **25**, 6464–6474.

[26] Deevi R, Fatehullah A, Jagan I, Nagaraju M, Bingham V, and Campbell FC (2011). PTEN regulates colorectal epithelial apoptosis through Cdc42 signalling. *Br J Cancer* **105**, 1313–1321.

[27] Standaert ML, Bandyopadhyay G, Kanoh Y, Sajan MP, and Farese RV (2001). Insulin and $PIP_3$ activate PKC-ζ by mechanisms that are both dependent and independent of phosphorylation of activation loop (T410) and autophosphorylation (T560) sites. *Biochemistry* **40**, 249–255.

[28] Kim M, Datta A, Brakeman P, Yu W, and Mostov KE (2007). Polarity proteins PAR6 and aPKC regulate cell death through GSK-3β in 3D epithelial morphogenesis. *J Cell Sci* **120**, 2309–2317.

[29] Lorimer IA, Parolin DA, and Lavictoire SJ (2002). Induction of apoptosis in glioblastoma cells by an atypical protein kinase C pseudosubstrate peptide. *Anticancer Res* **22**, 623–631.
[30] Wang Q, Wang X, Hernandez A, Kim S, and Evers BM (2001). Inhibition of the phosphatidylinositol 3-kinase pathway contributes to HT29 and Caco-2 intestinal cell differentiation. *Gastroenterology* **120**, 1381–1392.
[31] Bai Z, Zhang Z, Ye Y, and Wang S (2010). Sodium butyrate induces differentiation of gastric cancer cells to intestinal cells via the PTEN/phosphoinositide 3-kinase pathway. *Cell Biol Int* **34**, 1141–1145.
[32] Heo KS, Lee H, Nigro P, Thomas T, Le NT, Chang E, McClain C, Reinhart-King CA, King MR, Berk BC, et al. (2011). PKCζ mediates disturbed flow-induced endothelial apoptosis via p53 SUMOylation. *J Cell Biol* **193**, 867–884.
[33] Jass JR, Atkin WS, Cuzick J, Bussey HJ, Morson BC, Northover JM, and Todd IP (2002). The grading of rectal cancer: historical perspectives and a multivariate analysis of 447 cases. *Histopathology* **41**, 59–81.
[34] Busacca S, Sheaff M, Arthur K, Gray SG, O'Byrne KJ, Richard DJ, Soltermann A, Opitz I, Pass H, Harkin DP, et al. (2012). BRCA1 is an essential mediator of vinorelbine-induced apoptosis in mesothelioma. *J Pathol* **227**, 200–208.
[35] Hayashi Y, Molina JR, Hamilton SR, and Georgescu MM (2010). NHERF1/EBP50 is a new marker in colorectal cancer. *Neoplasia* **12**, 1013–1022.
[36] Durden DA (2011). Evaluation of the order of hierarchical structures for the calculation of method uncertainty using nested and other designs. *J AOAC Int* **94**, 1643–1649.
[37] Lee JO, Yang H, Georgescu MM, Di Cristofano A, Maehama T, Shi Y, Dixon JE, Pandolfi P, and Pavletich NP (1999). Crystal structure of the PTEN tumor suppressor: implications for its phosphoinositide phosphatase activity and membrane association. *Cell* **99**, 323–334.
[38] Maehama T and Dixon JE (1999). PTEN: a tumour suppressor that functions as a phospholipid phosphatase. *Trends Cell Biol* **9**, 125–128.
[39] Corbalán-García S and Gómez-Fernández JC (2010). The C2 domains of classical and novel PKCs as versatile decoders of membrane signals. *Biofactors* **36**, 1–7.
[40] Raftopoulou M (2004). Regulation of cell migration by the C2 domain of the tumor suppressor PTEN. *Science* **303**, 1179–1181.
[41] Leslie NR, Yang X, Downes CP, and Weijer CJ (2007). PtdIns(3,4,5)$P_3$-dependent and -independent roles for PTEN in the control of cell migration. *Curr Biol* **17**, 115–125.
[42] Gálvez-Santisteban M, Rodriguez-Fraticelli AE, Bryant DM, Vergarajauregui S, Yasuda T, Bañon-Rodríguez I, Bernascone I, Datta A, Spivak N, Young K, et al. (2012). Synaptotagmin-like proteins control the formation of a single apical membrane domain in epithelial cells. *Nat Cell Biol* **14**, 838–849.
[43] Rescher U and Gerke V (2004). Annexins—unique membrane binding proteins with diverse functions. *J Cell Sci* **117**, 2631–2639.
[44] Wedlich-Soldner R, Altschuler S, Wu L, and Li R (2003). Spontaneous cell polarization through actomyosin-based delivery of the Cdc42 GTPase. *Science* **299**, 1231–1235.
[45] Irazoqui JE, Gladfelter AS, and Lew DJ (2003). Scaffold-mediated symmetry breaking by Cdc42p. *Nat Cell Biol* **5**, 1062–1070.
[46] Qin Y, Meisen WH, Hao Y, and Macara IG (2010). Tuba, a Cdc42 GEF, is required for polarized spindle orientation during epithelial cyst formation. *J Cell Biol* **189**, 661–669.
[47] Fairn GD, Hermansson M, Somerharju P, and Grinstein S (2011). Phosphatidylserine is polarized and required for proper Cdc42 localization and for development of cell polarity. *Nat Cell Biol* **13**, 1424–1430.
[48] Lima-Fernandes E, Enslen H, Camand E, Kotelevets L, Boularan C, Achour L, Benmerah A, Gibson LC, Baillie GS, Pitcher JA, et al. (2011). Distinct functional outputs of PTEN signalling are controlled by dynamic association with β-arrestins. *EMBO J* **30**, 2557–2568.
[49] Houslay MD (2011). Arresting times for PTEN. *EMBO J* **30**, 2513–2515.
[50] Anthony DF, Sin YY, Vadrevu S, Advant N, Day JP, Byrne AM, Lynch MJ, Milligan G, Houslay MD, and Baillie GS (2011). β-Arrestin 1 inhibits the GTPase-activating protein function of ARHGAP21, promoting activation of RhoA following angiotensin II type 1A receptor stimulation. *Mol Cell Biol* **31**, 1066–1075.
[51] Dubois T and Chavrier P (2005). ARHGAP10, a novel RhoGAP at the crossroad between ARF1 and Cdc42 pathways, regulates Arp2/3 complex and actin dynamics on Golgi membranes. *Med Sci (Paris)* **21**, 692–694.
[52] Hehnly H, Longhini KM, Chen JL, and Stamnes M (2009). Retrograde Shiga toxin trafficking is regulated by ARHGAP21 and Cdc42. *Mol Biol Cell* **20**, 4303–4312.
[53] Sampaio JL, Gerl MJ, Klose C, Ejsing CS, Beug H, Simons K, and Shevchenko A (2011). Membrane lipidome of an epithelial cell line. *Proc Natl Acad Sci USA* **108**, 1903–1907.
[54] Hoessli DC, Ilangumaran S, Soltermann A, Robinson PJ, Borisch B, and Nasir Ud D (2000). Signaling through sphingolipid microdomains of the plasma membrane: the concept of signaling platform. *Glycoconj J* **17**, 191–197.
[55] Gao X, Lowry PR, Zhou X, Depry C, Wei Z, Wong GW, and Zhang J (2011). PI3K/Akt signaling requires spatial compartmentalization in plasma membrane microdomains. *Proc Natl Acad Sci USA* **108**, 14509–14514.
[56] Li X, Leu S, Cheong A, Zhang H, Baibakov B, Shih C, Birnbaum MJ, and Donowitz M (2004). Akt2, phosphatidylinositol 3-kinase, and PTEN are in lipid rafts of intestinal cells: role in absorption and differentiation. *Gastroenterology* **126**, 122–135.
[57] Vandromme M, Rochat A, Meier R, Carnac G, Besser D, Hemmings BA, Fernandez A, and Lamb NJ (2001). Protein kinase B β/Akt2 plays a specific role in muscle differentiation. *J Biol Chem* **276**, 8173–8179.
[58] Hinderliter A, Almeida PF, Creutz CE, and Biltonen RL (2001). Domain formation in a fluid mixed lipid bilayer modulated through binding of the C2 protein motif. *Biochemistry* **40**, 4181–4191.
[59] Xu R, Boudreau A, and Bissell MJ (2009). Tissue architecture and function: dynamic reciprocity via extra- and intra-cellular matrices. *Cancer Metastasis Rev* **28**, 167–176.
[60] Horikoshi Y, Suzuki A, Yamanaka T, Sasaki K, Mizuno K, Sawada H, Yonemura S, and Ohno S (2009). Interaction between PAR-3 and the aPKC–PAR-6 complex is indispensable for apical domain development of epithelial cells. *J Cell Sci* **122**, 1595–1606.
[61] Whyte J, Thornton L, McNally S, McCarthy S, Lanigan F, Gallagher WM, Stein T, and Martin F (2010). PKCζ regulates cell polarisation and proliferation restriction during mammary acinus formation. *J Cell Sci* **123**, 3316–3328.
[62] Wald FA, Oriolo AS, Mashukova A, Fregien NL, Langshaw AH, and Salas PJ (2008). Atypical protein kinase C (iota) activates ezrin in the apical domain of intestinal epithelial cells. *J Cell Sci* **121**, 644–654.
[63] Liu H, Wu Z, Shi X, Li W, Liu C, Wang D, Ye X, Liu L, Na J, Cheng H, et al. (2013). Atypical PKC, regulated by Rho GTPases and Mek/Erk, phosphorylates Ezrin during eight-cell embryocompaction. *Dev Biol* **375**, 13–22.
[64] Li J, Dai Z, Jana D, Callaway DJ, and Bu Z (2005). Ezrin controls the macromolecular complexes formed between an adapter protein $Na^+/H^+$ exchanger regulatory factor and the cystic fibrosis transmembrane conductance regulator. *J Biol Chem* **280**, 37634–37643.
[65] Morales FC, Takahashi Y, Kreimann EL, and Georgescu MM (2004). Ezrin-radixin-moesin (ERM)-binding phosphoprotein 50 organizes ERM proteins at the apical membrane of polarized epithelia. *Proc Natl Acad Sci USA* **101**, 17705–17710.
[66] Mariadason JM, Rickard KL, Barkla DH, Augenlicht LH, and Gibson PR (2000). Divergent phenotypic patterns and commitment to apoptosis of Caco-2 cells during spontaneous and butyrate-induced differentiation. *J Cell Physiol* **183**, 347–354.
[67] Donohoe DR, Garge N, Zhang X, Sun W, O'Connell TM, Bunger MK, and Bultman SJ (2011). The microbiome and butyrate regulate energy metabolism and autophagy in the mammalian colon. *Cell Metab* **13**, 517–526.